Materials Science-Poland, 37(3), 2019, pp. 426-436
http://www.materialsscience.pwr.wroc.pl/
DOI: 10.2478/msp-2019-0051

sciendo

Synthesis and characterization of binary and ternary nanocomposites based on TiO_2, SiO_2 and ZnO with PVA based template-free gel combustion method

ELHAM FAKOORI[1], HASSAN KARAMI[1,2,*], AZIZOLLAH NEZHADALI[1]

[1]Department of Chemistry, Payamr Noor University, P. O. Box 19395-3697, Tehran, Iran
[2]Nano Research Laboratory, Department of Chemistry, Payame Noor University, Abhar, Iran

Binary and ternary nanocomposites based on TiO_2, SiO_2 and ZnO were synthesized by PVA-based template-free gel combustion method. The morphology and the particles sizes of the synthesized samples depended on some parameters including the initial concentrations of metal salts and PVA amount in the sol, solvent composition and solution pH. Effects of these parameters were investigated and optimized by using the Taguchi method. In the experimental design, the Taguchi L_{25} array was used to investigate six factors at five levels. The samples were characterized by dynamic light scattering (DLS), transmission electron microscopy (TEM), Brunauer-Emmett-Teller (BET) specific surface areas, scanning electron microscopy (SEM). The obtained results showed that the present method can be used to synthesize $TiO_2/SiO_2/ZnO$ ternary nanocomposite with an effective surface area of 0.3 $m^2 \cdot g^{-1}$ and ZnO/TiO_2, TiO_2/SiO_2, ZnO/SiO_2 binary nanocomposites with an effective surface area of 234 $m^2 \cdot g^{-1}$, 6 $m^2 \cdot g^{-1}$ and 0.5 $m^2 \cdot g^{-1}$, respectively. The ZnO/TiO_2 nanocomposite which was synthesized under the following experimental conditions: 2.5 wt.% Zn salt, 2.5 wt.% Ti salt, 2.0 wt.% PVA, pH = 1 and ethanol:water ratio 30:70 was selected by the Taguchi method as an optimum sample with the smallest particles (average diameter = 50 nm).

Keywords: *$TiO_2/SiO_2/ZnO$ nanocomposite; sol-gel method; pyrolysis; experimental design; Taguchi method*

1. Introduction

2. Introduction

In the last 20 years, the development of nanomaterials has primarily focused on single-component materials [1–3]. Since 2009, much attention has been paid to improve the properties of nanomaterials such as chemical reactivity, optical, electrical and magnetic properties which led to synthesize the nanocomposites with two or more components [4–6]. Among these systems, inorganic hetro-nanoparticles have become popular because, their quantum yields and photoluminescence tend to increase according to the quantum confinement effect [7] therefore, making them applicable for use in solar cells and photocatalyst systems [8, 9]. In recent years, there have been a great interest in metal oxide nanoparticles because of their special electronic and chemical properties. Some of metal oxide nanoparticles such as TiO_2, Al_2O_3, ZnO, SiO_2 and CuO possess photocatalytic, electrical conductivity and UV absorption properties. Nowadays, intensive studies on metal oxide nanoparticles have been focusing on three special properties antimicrobial, UV blocking and self-decontamination for civilian health products and military protection gears [10]. As a promising compound, titania (TiO_2) has been widely used in the photocatalytic degradation of organic pollutants of water and air [11–13]. Pure TiO_2 has energy gap of 3.2 eV, thus, UV light is necessary to excite electrons on the TiO_2 surface. To activate the photocatalyst with higher efficiency and longer wavelength, a number of techniques have been introduced. One strategy is to prepare TiO_2/metal oxide nanocomposites such as SiO_2/TiO_2 [14], CdS/TiO_2 [15], ZnO/TiO_2 [16] and SnO_2/TiO_2 [17]. Lifetime of photo-induced charge carries is a main factor for improving

*E-mail: karami_h@yahoo.com

photocatalytic activity. As for ZnO-TiO_2 [18], the electron transfers from the conduction band of ZnO to that of TiO_2 under illumination, and conversely, the holes transfer from the valence band of TiO_2 to that of ZnO. Thus, the lifetime of photoinduced pairs increases since their recombination rate decreases. In order to extend the range of excitation energies of TiO_2 into the visible region, materials of the narrow band gap, such as ZnO, have been coupled with TiO_2 [19–22]. Since 2004, much attention has been paid to the synthesis of nanosilica because of its easy preparation and wide industrial applications, such as catalysis, pigments, pharmacy, electronic and thin film substrates, electronic and thermal insulators, and humidity sensors [23]. The silica particles play a different role in each of the above applications. The quality of these products is highly dependent on the size and size distribution of the particles [24]. Stöber et al. [25] reported in 1968 a pioneering method for the synthesis of spherical and monodisperse silica nanoparticles from aqueous alcohol solutions of silicon alkoxides in the presence of ammonia as a catalyst, and different sizes of silica nanoparticles ranging from 50 nm to 1 μm with a narrow size distribution were prepared. The sol-gel approach is one of the most important methods for the preparing of high quality nano-SiO_2 powders [26]. The sol-gel techniques are the most effective and popular for the preparation of metal oxide and metal/organic nanocomposites [27–34]. Karami et al. [35] introduced PVA- based sol-gel combustion method to prepare metal oxide and metal oxide nanocomposites. Nanocomposites are materials which are prepared by combining two or more pure substances with distinctly different mechanical, electrical, magnetic, optical, thermal, or chemical properties in order to create a composite material that combines the desirable properties of each other to create a multi-functional substance. Nanosized crystalline TiO_2 and SiO_2/TiO_2 mixed oxide particles were synthesized and used as photocatalyst for the degradation of rhodamine B [36]. TiO_2/SiO_2 composites are very promising in the field of heterogeneous photocatalysis, since they could provide simultaneously enhanced photocatalytic and thermal properties compared to pure TiO_2 photocatalyst [37–40]. It has been reported that photocatalytic reactivity of TiO_2/SiO_2 nanocomposites is highly dependent on the Ti/Si ratio [41–44]. The aim of this work is to synthesize the TiO_2/SiO_2/ZnO binary and ternary nanocomposites by the PVA-based sol-gel combustion method which was introduced in [35]. The experimental synthesis conditions were investigated using Taguchi design.

3. Experimental

3.1. Material

The used chemicals included titanyl sulfate (TS), zinc chloride (ZC), sodium metasilicate (SMS), polyvinyl alcohol (PVA) and absolute ethanol (Et) with reagent grade, which were purchased from Merck and were used without additional purification. Double-distilled water (W) was used in all the experiments.

3.2. Instrumental

A scanning electron microscope with EDX detector from Philips Co. (XL30) was used for studying of morphology, particle size, and performing surface analysis of the prepared nanocomposite powders. X-ray diffraction (XRD) studies were carried out using a Decker D8 instrument. A JEOL-200 CX transmission electron microscope was used to obtain micrographs. Size distribution diagrams of the samples were obtained by DLS (Malvern Instruments Ltd., Zetasizer Ver. 6.32). The specific surface area was calculated from measurements of N_2 adsorption/desorption using Nova 2000 series Chromatech apparatus at 77 K.

3.3. Procedures

3.3.1. Design of experiments

To optimize experimental parameters for synthesizing TiO_2/SiO_2/ZnO nanocomposites, a Taguchi experimental design approach was applied. To design the experiments, the following steps were used:

1. Statement of problems and objective of the experiments.

2. Identification of factors and interactions.
3. Choice of factor levels.
4. Selection of orthogonal array.
5. Assignment of factors.
6. Experimental setup.
7. Statistical data analysis. Interpretation and experimental conclusion.

Taguchi method was applied with the objective of achieving nanocomposite with minimum particle size and the biggest length/diameter ratio, thus a function of particle diameter and length/diameter ratio was considered as the response (Z score). The six parameters identified as processing factors affecting the particle size included titanium salt, zinc salt, silicon salt, PVA, pH, and solvent composition. The synthesis parameters (X) were analyzed in five selected levels. The factors and selected levels are shown in Table 1. To analyze the significance of each factor, an L_{25} orthogonal array was chosen with five logical levels for each parameter (Table 2).

In the experiments, the factors and levels were used to design an L_{25} orthogonal array (Table 3). Minitab software (version 16) was used for the statistical calculations.

3.3.2. Synthesis procedure

In this procedure, the amount of variables was used according to Taguchi design. The specified amounts of three initial salts and PVA were dissolved in an ethanol/water mixed solvent with different ratios and at different pHs. The mixture was heated up to 70 °C to from a homogeneous and transparent sol then, the sol was heated up to 100 °C to evaporate the solvent and form a hard homogenous gel. The black gel was pyrolyzed in electrical furnace at 700 °C for 4 hours.

During the pyrolysis, the outer surface of PVA polymeric network was slowly burnt and the salts content was calcined and converted into composite nanoparticles. The obtained samples were crushed to prepare a fine powder. The morphology, particles sizes, and the chemical composition of the samples were analyzed by the SEM, TEM, BET and DLS.

In this procedure, there are some parameters, such as zinc, titanium and silicon salts, PVA, solvent composition, and solution pH, which can effect the morphology and particles size of the final powder. The effects of all parameters were studied by Taguchi method.

4. Results and discussion

In the PVA-based sol-gel combustion method, PVA linear chains are connected to each other to form three-dimensional polymeric network during the process of converting the sol to gel. The formed network is rigid and contains a large number of regular cavities. If zinc, silicon and titanium salts are present in the sol, these salts are homogeneously distributed in regular gel cavities. In each gel cavity, only a limited number of salt molecules can be present. The location of the dispersed molecules in the gel network is fixed and the dispersed molecules in the gel network cannot alter their positions [35]. In the pyrolysis of the gel, the outer layers of the gel first burn and the salts inside the cavities of the outer layers of the gel are released, clacined and converted into nanocomposite particles. The morphology of the formed nanocomposite particles depends on the shape of gel cavities as well as pyrolysis rate and temperature. The size of final particles depends on the size of cavities in gel as well as other pyrolysis parameters. The rigidity of the gel network prevents mixing of salt inside a cavity with those of the other cavity.

4.1. Taguchi optimization methodology

In this method, the amounts of three salts (TS, ZC and SMS), PVA, the composition of solvent, and pH can affect the morphology and the particles size of the final nanocomposite. Therefore, the amounts of these parameters were optimized by the Taguchi method. Based on this experimental design, 25 samples were synthesized to identify the effect of the mentioned variables on the composition, morphology and particles size of the nanocomposite samples. Table 3 shows the experimental conditions of the synthesized samples in the optimized set.

Table 1. Studied parameters (X) and their levels*.

Design parameter	Level 1	Level 2	Level 3	Level 4	Level 5
TS % (X_1)	0	1.25	2.5	3.75	4.75
SMS % (X_2)	0	1.25	2.5	3.75	4.75
ZC % (X_3)	0	1.25	2.5	3.75	4.75
PVA % (X_4)	0	0.5	1	1.5	2
pH (X_5)	0	1	2.5	3.5	4.5
Solvent composition (X_6)*	100 W	10 W + 90 Et	30 W + 70 Et	70 W + 30 Et	50 W + 50 Et

*All numbers are expressed in percentage terms. **W = water, Et = ethanol.

Table 2. L_{25} orthogonal array of Taguchi method.

Sample No.	P1	P2	P3	P4	P5	P6	Sample No.	P1	P2	P3	P4	P5	P6
1	1	1	1	1	1	1	14	3	4	1	3	5	2
2	1	2	2	2	2	2	15	3	5	2	4	1	3
3	1	3	3	3	3	3	16	4	1	4	2	5	3
4	1	4	4	4	4	4	17	4	2	5	3	1	4
5	1	5	5	5	5	5	18	4	3	1	4	2	5
6	2	1	2	3	4	5	19	4	4	2	5	3	1
7	2	2	3	4	5	1	20	4	5	3	1	4	2
8	2	3	4	5	1	2	21	5	1	5	4	3	2
9	2	4	5	1	2	3	22	5	2	1	5	4	3
10	2	5	1	2	3	4	23	5	3	2	1	5	4
11	3	1	3	5	2	4	24	5	4	3	2	1	5
12	3	2	4	1	3	5	25	5	5	4	3	2	1
13	3	3	5	2	4	1							

Each experiment was conducted two times. The average diameter and length of the sample particles were measured and Z score (Z = D + 3D/L) was defined as a function of diameter D and length L of particles based on SEM images. The SEM images of 25 samples were classified into 5 groups based on TS level (Fig. 1 to Fig. 5).

All samples in Fig. 1 are binary ZnO/SiO_2 nanocomposites with ZC/SMS ratio 1. They were synthesized in the absence of TS and at different values of PVA and pH. Fig. 1 shows that all the samples include nanoparticles in semi-rod shape but sample 4 includes rectangular nanosheets of binary ZnO/SiO_2 nanocomposite. It is expected that sample 4 has high surface area. Therefore, it was selected for further characterizations. Fig. 2 shows SEM images of 5 samples synthesized at the same TS level (1.25 %) and different ZC levels. The SMS level increased from 0 % to 4.75 % in sample 6 to 10. The morphology of the final sample is changing from sea stone shapes to amorphous porous structures.

Fig. 3 shows SEM images of sample 11 to sample 15 at TS level 3 (2.5 %). Based on the SEM image of sample 11, the absence of SMS resulted in forming crystalline ZnO/TiO_2 nanocomposite. Sample 11 has the most uniform structure and the smallest particles. Therefore, it was selected for further characterization. The presence of SMS resulted in forming amorphous porous structures (sample 14 and sample 15).

Table 3. Experimental design (factors and levels) used in the orthogonal L_{25}.

Sample No.	TS % (X_1)	SMS % (X_2)	ZC % (X_3)	PVA % (X_4)	pH (X_5)	Solvent composition (X6)	Sample No.	TS % (X_1)	SMS % (X_2)	ZC % (X_3)	PVA % (X_4)	pH (X_5)	Solvent composition (X6)
1	0	0	0	0	0	0	14	2.5	3.75	0	1	4.5	90 Et + 10 W
2	0	1.25	1.25	0.5	1	90 Et + 10 W	15	2.5	4.75	1.25	1.5	0	70 Et + 30 W
3	0	2.5	2.5	1	2.5	70 Et + 30 W	16	3.75	0	3.75	0.5	4.5	70 Et + 30 W
4	0	3.75	3.75	1.5	3.5	30 Et + 70 W	17	3.75	1.25	4.75	1.5	0	30 Et + 70 W
5	0	4.75	4.75	2	4.5	50 Et + 50 W	18	3.75	2.5	0	1.5	1	50 Et + 50 W
6	1.25	0	1.25	1	3.5	50 Et + 50 W	19	3.75	3.75	1.25	2	2.5	100 W
7	1.25	1.25	2.5	1.5	4.5	100 W	20	3.75	4.75	2.5	0	3.5	90 Et + 10 W
8	1.25	2.5	3.75	2	0	90 Et + 10 W	21	4.75	0	4.75	1.5	2.5	90 Et + 10 W
9	1.25	3.75	4.75	0	1	70 Et + 30 W	22	4.75	1.25	0	2	3.5	70 Et + 30 W
10	1.25	4.75	0	0.5	2.5	30 Et + 70 W	23	4.75	2.5	1.25	0	4.5	30 Et + 70 W
11	2.5	0	2.5	2	1	30 Et + 70 W	24	4.75	3.75	2.5	0.5	0	50 Et + 50 W
12	2.5	1.25	3.75	0	2.5	50 Et + 50 W	25	4.75	4.75	3.75	1	1	100 W
13	2.5	2.5	4.75	0.5	3.5	100 W							

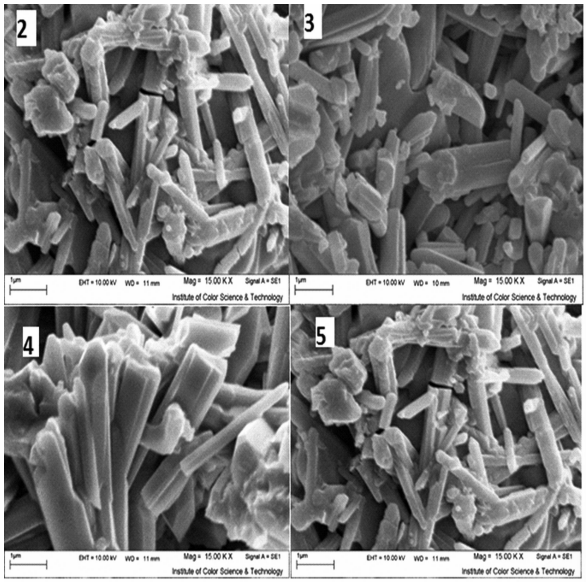

Fig. 1. SEM images of the prepared nanocomposites with TS content at the level 1. All numbers in the images are sample numbers according to Table 3 (sample 2 to sample 5).

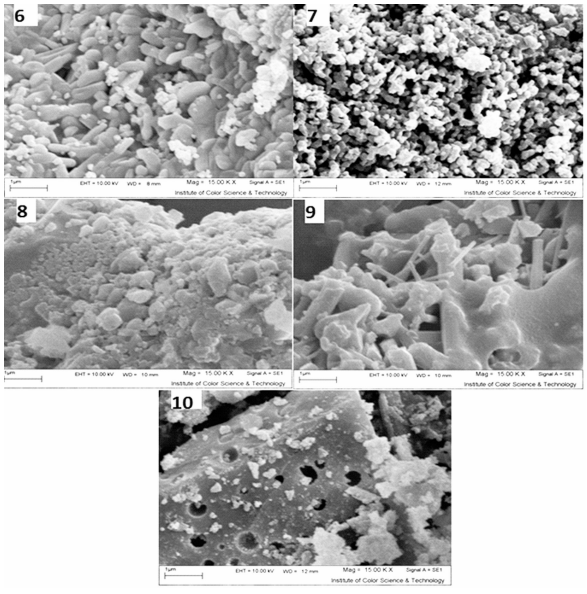

Fig. 2. SEM images of the prepared nanocomposite with TS content at the level 2. All numbers in the images are sample numbers according to Table 3 (sample 6 to sample 10).

Fig. 4 shows SEM images of sample 16 to sample 20 at TS level 4 (3.75 %). Sample 17 and sample 18 include more uniform and smaller particles than other samples in Fig. 4. Sample 17 and sample 18, which included ternary $ZnO/TiO_2/SiO_2$ nanocomposite and binary TiO_2/SiO_2 nanocomposite, were selected for further characterization respectively. Sample 21

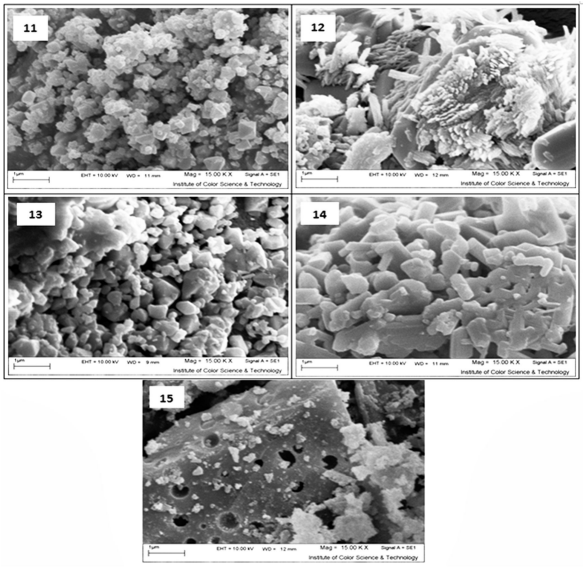

Fig. 3. SEM images of the prepared nanocomposite with TS content at the level 3. All numbers in the images are sample numbers according to Table 3 (sample 11 to sample 15).

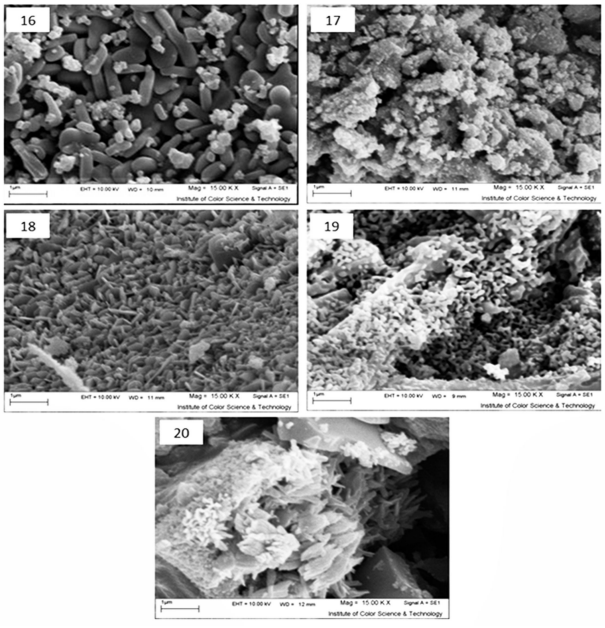

Fig. 4. SEM images of the prepared nanocomposites with TS content at the level 4. All numbers in the images are sample numbers according to Table 3 (sample 16 to sample 20).

to sample 25 were synthesized at TS level 5 (Fig. 5). Based on SEM images in Fig. 4 and Fig. 5, the morphologies of sample 17 and sample 24 are similar because, according to Table 3, sample 17 and sample 24 were synthesized at the same pH (pH = 0). Based on the SEM images of 25 samples in Fig. 1 to Fig. 5, any change in each of the selected factors (the amount of salts, amount of PVA, pH and solvent composition) can change the morphology and the particle size of the samples. Based on Fig. 1 to Fig. 5 (SEM images of sample 2 to sample 25), the followings conclusions can be drawn:

1. The presence of zinc chloride (ZC) in the initial sol results in forming nanorod composite.
2. The presence of sodium metasilicate (SMS) at level 4 and level 5 in the initial sol makes amorphous nanocomposites.
3. pH has a significant effect on the morphology and the particle size of nanocomposites.
4. The presence of titanyl sulfate (TS) in the samples causes a decrease in nanorods in the final nanocomposites.

Sample 17, as a selected ternary nanocomposite was analyzed by XRD (Fig. 6). The presented XRD patterns confirm the presence of zinc, titanium and silicon oxides in the synthesized nanocomposite. Debye-Scherrer equation 1 was applied for the biggest diffraction peak of the sample to calculate the crystallite size [45]:

$$D = \frac{0.94\lambda}{\beta \cos\theta} \tag{1}$$

where λ is the wavelength of X-ray (0.154056 nm), β is the full width of the peak at half maximum height and θ is the angle of radiation. The average size of nanocomposite particles was calculated about 82 nm. To select the optimum sample based on Z score, the concept of "the small is the better" was used. In this manner, S:N ratio for each sample was calculated using equation 2 [4]:

$$\frac{S}{N} = -10\log\frac{1}{n}\sum_{i}^{n} y_i^2 \tag{2}$$

where y_i is the characteristic property (Z score) and n is the number of replication. Fig. 7 shows

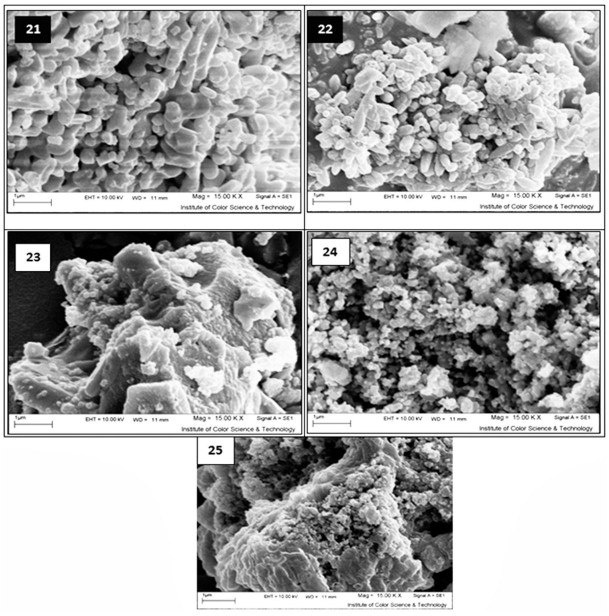

Fig. 5. SEM images of the prepared nanocomposite with TS content at the level 5. All numbers in the images are sample numbers according to Table 3 (sample 21 to sample 25).

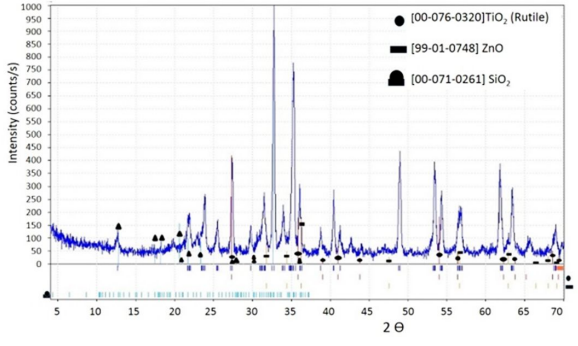

Fig. 6. Relationship between S:N values and the control parameters.

the results of S:N analysis of all samples. The higher S:N ratio shows the positive effect of each factor on the decreasing of Z score. Therefore, the optimum level of each factor can be achieved at the biggest S:N. It should be mentioned that all amounts of S:N are negative. Therefore, –50.38 is the biggest S:N ratio.

In Fig. 7, the difference between the maximum and minimum values of each factor can be related to their effect on S:N ratio. The summary results of S:N calculations are presented in Table 4. Based

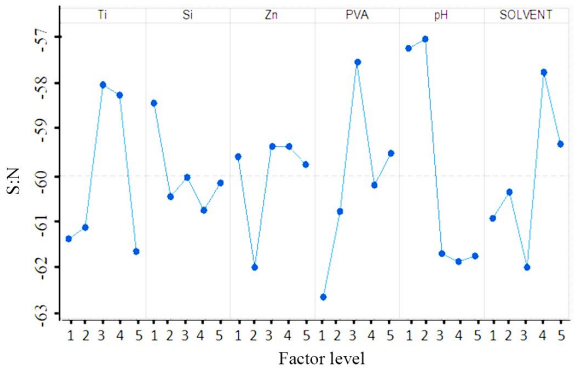

Fig. 7. XRD patterns of $ZnO/TiO_2/SiO_2$ nanocomposites.

on the data presented in Table 4 and Fig. 7, the optimum conditions to obtain the smallest particles are as follows: Ti and Zn salts 2.5 g (level 3), Si salt 0 g (level 1), PVA 2 g (level 5), pH 1 (level 2) and solvent ratio ethanol:water 30:70 (level 4). These results confirm that the particle size in the prepared nanocomposites was significantly influenced by the amount of the initial processing parameters. A confirmation run was performed under the selected optimal conditions to check the average particle size. Table 5 shows the optimum synthesis conditions and the amounts of the experimental and predicted Z scores. There is a good agreement between the predicted and experimental Z scores.

Furthermore, the results of variance analysis (ANOVA) are shown in Table 6. The relative contribution percentage P and F-values of each factor were obtained by the ANOVA method and are given in Table 6. It can be concluded that there is a significant difference between the effects of the investigated factors. The obtained order of importance is: pH, Ti salt, Si and Zn salts, solvent composition, and PVA amount.

The three-dimensional response surface plots were used to explain the interactions between variables and to find the optimum level of each variable for the synthesis of a nanocomposite with the smallest particles. For the 15 possible two-variables combination interaction (X_1X_2, X_1X_3, X_1X_4, X_1X_5, X_1X_6, X_2X_3, X_2X_4, X_2X_5, X_2X_6, X_3X_4, X_3X_5, X_3X_6, X_4X_5, X_4X_6 and X_5X_6), 15 response surface plots were drawn and shown

Table 4. The S:N ratio for the studied samples.

Experiment	Z_1	Z_2	$Z_{average}$	S:N	Experiment	Z_1	Z_2	$Z_{average}$	S:N
1	0	0	0	0	14	750	834	792	–57.9745
2	1200	1200.2	1200.1	–61.58	15	997	1017	1007	–60.0606
3	1190	1210	1200	–61.5836	16	1154	1030	1092	–60.7645
4	1108.42	1112	1110.21	–60.9081	17	350	402	376	–51.5038
5	1180	1189.8	1185	–61.4744	18	500	556	528	–54.4527
6	1020.8	1080	1050.4	–60.4271	19	1358	1402	1380	–62.7976
7	1470	1530	1500.0	–63.5270	20	1200	1320	1260	–62.0074
8	800	802	801	–58.0727	21	1290	1304	1297	–62.2588
9	1368	1332.4	1350.2	–62.6080	22	1751	1791	1771	–64.9644
10	1157.82	1100	1128.91	–61.0532	23	1790	1812	1801	–65.1103
11	328.25	332.75	330.5	–50.3834	24	966	930.6	948.3	–59.5389
12	1050	1150.8	1100.4	–60.8310	25	653	667	660	–56.3909
13	1123	1137	1130	–61.0616					

Table 5. The experimental synthesis conditions and the experimental and predicted Z cores.

results		solvent	pH	PVA [g]	SMS [g]	ZC [g]	TS [g]	Sample No.
$Z_{Predicted}$	$Z_{Experiment}$	30 Et + 70 W	1‘	2	0	2.5	2.5	11
230‘	240.4							

in Fig. 8 (X_1, X_2, X_3, X_4, X_5 and X_6 were introduced in Table 3).

Fig. 8a to Fig. 8e show the interactive effects of TS amount (X_1) and other synthesis factors (X_2, X_3, X_4, X_5 and X_6) on the response (Z_{score}). These plots show that the TS level 3 (2.5 wt.%) is the best to synthesize the smallest particles. The variations in the amounts of other factors cannot change the optimum amount of TS level. Fig. 8f to Fig. 8h are the plots of interactive combinations of ZC level (X3) with solvent composition (X_6), pH level (X_5) and PVA level (X_4). The optimum of ZC is level 3 (2.5 wt.%) in combination with other factors. Fig. 8i to Fig. 8l show that the presence of SMS in the initial sol causes an increase in the average particles size. Therefore, in the absence of SMS (SMS level 1), a binary TiO_2/ZnO nanocomposite with the smallest particles can be synthesized. To synthesize the ternary TiO_2/SiO_2/ZnO nanocomposite with the smallest particles, the level of SMS should be kept at level 2 (1.25 wt.%). Fig. 8m and Fig. 8n are the plots for the interaction effects of PVA with solvent and pH. Based on Fig. 8m and Fig. 8n, the optimum amount of PVA in all combinations is 2 wt.% (level 5). Fig. 8o shows that the optimum levels of solvent composition and pH are 4 (30 % Et + 70 % W) and 2 (pH = 1), respectively. Based on the presented data in Fig. 8, experiment 11 and experiment 17 in Table 3 can be used as optimum conditions to synthesize binary TiO_2/ZnO nanocomposite and ternary TiO_2/SiO_2/ZnO nanocomposite with the smallest particles sizes, respectively.

Based on the Langmuir surface area calculation, it was found that the sample has a biggest specific surface area of 233.5 $m^2 \cdot g^{-1}$.

Sample 11, as optimum binary TiO_2/ZnO nanocomposite was analyzed by SEM, DLS, TEM and BET (Fig. 9). Fig. 9a (SEM image) shows the crystallinity of the sample. Fig. 9b shows TEM micrograph of the sample with 50 nm average

Table 6. Analysis of variance based on S:N ratios.

P-Value	F-Value	Adj MS	Adj SS	Contribution [%]	Seq SS	DF	Source
0.479	0.91	165433	661733	15.35	661733	4	Ti
0988	0.30	140968	563872	4.88	563872	4	Si
0.990	0.32	135279	541115	5.02	541115	4	Zn
0.810	1.09	78768	315071	17.2	315071	4	PVA
0.519	0.95	107367	429468	15.8	429468	4	Solvent
0.023	3.59	450265	1801059	41.77	1801059	4	pH

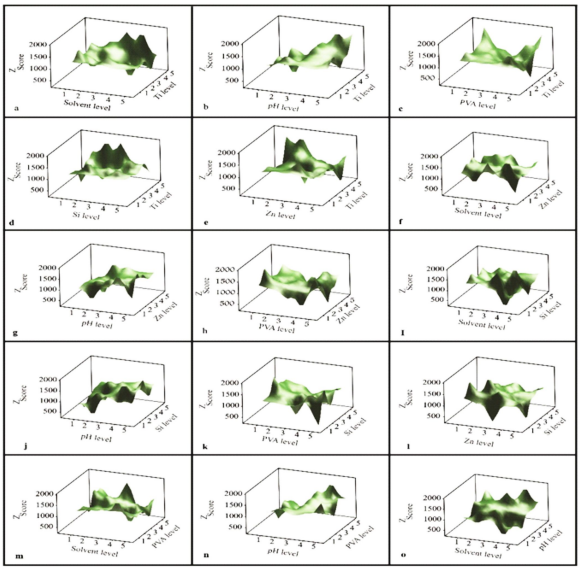

Fig. 8. Two variable 3D surface plots of synthesis factors; 15 different combinations were studied.

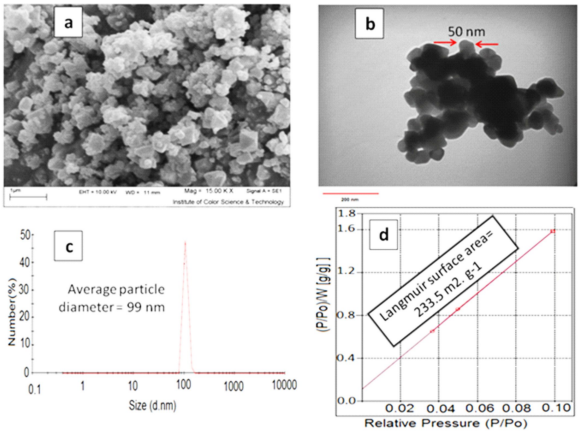

Fig. 9. SEM image (a), TEM micrograph (b), DLS diagram (c) and BET diagram (d) of the synthesized (optimized sample) TiO_2/ZnO nanocomposite.

diameter of the crystalline nanoparticles. Fig. 9c shows the size distribution of the sample in the range of 80 nm to 150 nm with average diameter of 99 nm. Fig. 9d shows the adsorption/desorption curves of N_2 gas for the binary nanocomposite.

It should be noted that the particles sizes of the sample obtained by DLS (using Malvern size analyzer) are bigger than those obtained by TEM. This is due to the calculation method of DLS which determines the particle size based on the laser scattering by the particles. The accuracy of measurement results may be affected by the conditions of sample dispersion in the used solvent. In contrast, the TEM results represent a direct observation of particle size and distribution within a local region. Thus, the TEM results tend to be smaller than those of the Malvern analyzer. However, the measurement results of the Malvern analyzer represent a larger sampling volume of nanocomposite suspension than that one of TEM measurement, and they can be used for evaluation. In general, it is suggested to include both types of the analysis for more accurate data interpretation.

The obtained results show that the present method can be used to synthesize TiO_2/SiO_2/ZnO ternary nanocomposite with an effective surface area of 0.3 $m^2 \cdot g^{-1}$ and binary nanocomposites ZnO/TiO_2, TiO_2/SiO_2, ZnO/SiO_2 with an effective surface area of 234 $m^2 \cdot g^{-1}$, 6 $m^2 \cdot g^{-1}$ and 0.5 $m^2 \cdot g^{-1}$, respectively. In addition, the adsorption-desorption analysis indicates that TiO_2/ZnO nanocomposite has a maximum surface

area compared with other nanocomposites.

5. Conclusions

It is concluded that the presented method is a new selective and template-free approach based on PVA gel pyrolysis for the synthesis of binary and ternary nanocomposites based on TiO_2, SiO_2 and ZnO. Taguchi experimental design can be successfully used to optimize the synthesis conditions of metal oxide nanocomposites with a simple experimental set. The obtained results showed that any variation in synthesis conditions results in a considerable change in the morphology and particle size of the nanocomposite sample. The presence of two metal salts in the initial composition enables obtaining a binary nanocomposite of the following metal oxides (ZnO/TiO_2, ZnO/SiO_2 or TiO_2/SiO_2) and also, the presence of three metal salts in the synthesis sol enables obtaining a ternary nanocomposite of the corresponding metal oxides ($TiO_2/ZnO/SiO_2$). The presence of zinc chloride in the synthesis sol results in forming rod shaped nanoparticles.

Acknowledgements

The authors would like to thank the financial support of this work by the Abhar Payame Noor University Research Council.

References

[1] WANG L., MUHAMMED M., *J. Mater. Chem.*, 9 (1999), 2871.
[2] MEULENKAMP E.A., *J. Phys. Chem. B*, 102 (1998), 5566.
[3] SONG Z., LI Q., GAO L., *J. Mater. Sci. Technol.*, 13 (1997), 321.
[4] ZHUANG J., LIU M., LIU H., *Sci. China B*, 52 (2009), 2125.
[5] USUI H., *Mater. Lett.*, 63 (2009), 1489.
[6] LI F., HUANG X., JIANG Y., LIU L., LI Z., *Mater. Res. Bull.*, 44 (2009), 437.
[7] KIM S., FISHER B., EISLER H.J., BAWENDI M., *J. Am. Chem. Soc.*, 125 (2003), 11466.
[8] TAK Y., HONG S.J., LEE J.S., YONG K., *J. Mater. Chem.*, 19 (2009), 5945.
[9] KIM C., CHOI M., JANG J., *Catal. Commun.*, 11 (2010), 378.
[10] RAHMAN I.A., PADVETTAN V., *J. Nanomater.*, (2012), 1. DOI: 10.1155/2012/132424.
[11] HOFFMANN M.R., MARTIN S.T., CHOI W., BAHNEMANN D.W., *Chem. Rev.*, 95 (1995), 69.
[12] WANG C., AO Y., WANG P., HOU J., QIAN J., ZHANG S., *J. Hazard. Mater.*, 178 (2010), 517.
[13] WANG C., AO Y., WANG P., HOU J., QIAN J., *Mater. Lett.*, 64 (2010), 1003.
[14] ARAI Y., TANAKA K., KHLAIFAT A.L., *J. Mol. Catal. A: Chem.*, 243 (2006), 85.
[15] BISWAS S., HOSSAIN M.F., TAKAHASHI T., KUBOTA Y., FUJISHIMA A., *Thin Solid Films*, 516 (2008), 7313.
[16] HOUŠKOVÁ V., ŠTENGL V., BAKARDJIEVA S., MURAFA N., *J. Phys. Chem. Solids*, 69 (2008), 1623.
[17] LEE H.C., HWANG W.S., *Appl. Surf. Sci.*, 253 (2006), 1889.
[18] SERPONE N., MARUTHAMUTHU P., PICHAT P., PELIZZETTI E., HIDAKA H., *J. Photochem. Photobiol. A: Chem.*, 85 (1995), 247.
[19] LIAO D.L., BADOUR C.A., LIAO B.Q., *J. Photochem. Photobiol. A: Chem.*, 194 (2008) 11.
[20] WANG J., JIANG Z., ZHANG L., KANG P., XIE Y., LV Y., ZHANG X., *Ultrason. Sonochem.*, 16 (2009), 225.
[21] XU X., WANG J., TIAN J., WANG X., DAI J., LIU X., *Ceram. Int.*, 37 (2011), 2201.
[22] JANITABAR-DARZI S., MAHJOUB A.R., *J. Alloy. Compd.*, 486 (2009), 805.
[23] GIESCHE H., *J. Eur. Ceram. Soc.*, 14 (1994), 205.
[24] VENKATATHRI N., *Bull. Mater. Sci.*, 30 (2007) 615.
[25] STÖBER W., FINK A., BOHN E., *J. Colloid Interface Sci.*, 26 (1968), 62.
[26] LINDBERG R., SJÖBLOM J., SUNDHOLM G., *Colloids Surf. A*, 99 (1995), 79.
[27] CHAN Y., ZIMMER J.P., STROH M., STECKEL J.S., JAIN R.K., BAWENDI M.G., *Adv. Mater.*, 16 (2004), 2092.
[28] EPIFANI M., GIANNINI C., TAPFER L., VASANELLI L., *J. Am. Ceram. Soc.*, 83 (2000), 2385.
[29] GONELLA F., MATTEI G., MAZZOLDI P., SADA C., BATTAGLI N.G., CATTARUZZA E., *Appl. Phys. Lett.*, 75 (1999) 55.
[30] LIZ-MARZÁN L.M., GIERSIG M., MULVANEY P., *Langmuir*, 12 (1996), 4329.
[31] HE J., ICHINOSE I., KUNITAKE T., NAKAO A., *Langmuir*, 18 (2002), 10005.
[32] SONG J.H, ATAY T., SHI S., URABE H., V. NURMIKKO A., *Nano Lett.*, 15 (2005), 1557.
[33] SHTER G.E., BEHAR-LEVY H., GELMAN V., GRADER G.S., AVNIR D., *Adv. Funct. Mater.*, 17 (2007), 913.
[34] TRAVERSA E., DI VONA M.L., LICOCCIA S., SACERDOTI M., CAROTTA M.C., CREMA L., MARTINELLI G., *J. Sol-Gel Sci. Technol.*, 22 (2001), 167.
[35] KARAMI H., AMIFAR A., TAVALLALI H., NAMDAE Z.A., *J. Clust. Sci.*, 21 (2011), 1.

[36] SAYILKAN F., ASILTURK M., SENER S., ERDEMOGLU S., ERDEMOGLU M., SAYILKAN H., *Turk. J. Chem.*, 31 (2007), 211.
[37] CALLEJA G., SERRANO D.P., SANZ R., PIZARRO P., *Microporous Mesoporous Mater.*, 111 (2008), 429.
[38] GARZELLA C., COMINI E., BONTEMPIL E., DEPEROL L.E., FRIGERI C., SBERVEGLIERI G., *Mater. Res. Soc. Symp. Proc.*, 638 (2001), 111.
[39] WANG Z., HELMERSSON U., KALL P., *Thin Solid Films*, 405 (2002), 50.
[40] IVANOVA T., HARIZANOVA A., SURTCHEV M., *Mater. Lett.*, 55 (2002), 327.
[41] DOHSHI S., TAKEUCHI M., ANPO M., *Catal. Today*, 85 (2003), 75.
[42] GONÇALVES R.R., MESSADDEQ Y., ATIK M., RIBEIRO S.J., *Mater. Res.*, 2 (1999), 11.
[43] NISHIDE T., SATO M., HARA H., *J. Mater. Sci.*, 35 (2000), 465.
[44] CABBRERA S., EL HASKOURI J., BELTRA'N-PORTER A., BELTRA'N-PORTER D., MARCOS M.D., AMORO'S P., *J. Solid State Sci*., 2 (2000) 513.
[45] ROSTAMKHANI F., KARAMI H., GHASEMI A., *Desalin. Water Treat.*, 60 (2017), 319.

Received 2018-06-13
Accepted 2018-11-08